Kristall und Technik	8	7	1973	785–801

N. J. J. Huige, M. M. G. Senden, H. A. C. Thijssen

Department of Physical Technology, Eindhoven University of Technology, Eindhoven, The Netherlands

Nucleation and Growth Kinetics for the Crystallization of Ice from Dextrose Solutions in a Continuous Stirred Tank Crystallizer with Supercooled Feed[1])

The crystallization of ice in aqueous dextrose solutions is studied in an adiabatic continuous stirred tank crystallizer with a supercooled feed stream. The effective diameter of the ice crystals was determined for various values of mean crystal residence time, feed supercooling, magma density, stirring rate, and dextrose concentration. For all process conditions the supercooling was measured at 9–12 different locations in the crystallizer. These local supercoolings were averaged algebraically to yield the bulksupercooling.

From the experimental results growth and nucleation rates have been calculated. By comparing the experimental growth rates to growth rates calculated by means of a mathematical model kinetics for the inbuilding of water molecules into the ice lattice have been determined. The growth rate appears to be directly proportional to the interface supercooling. The rate constant decreases exponentially with increasing weight percentage of dextrose in the solution.

The nucleation rate was found to be directly proportional to total crystal surface per unit volume of suspension and proportional to the bulksupercooling to the power 2.1. Nucleation is believed to occur by breakage of dendrites from the surface of parent crystals.

Die Kristallisation von Eis in wäßrigen Dextroselösungen wird in einem adiabatischen kontinuierlichen Rührkristallisator bei unterkühltem Zufluß der Mutterlösung untersucht. Der effektive Durchmesser der Eiskristalle wurde für verschiedene Werte der mittleren Verweilzeit der Kristalle, der Unterkühlung des Zuflusses, der Suspensionsdichte, der Rührgeschwindigkeit und der Dextrosekonzentration bestimmt. Für alle Bedingungen der Prozeßführung wurde die Unterkühlung an 9–12 verschiedenen Stellen des Kristallisators gemessen. Diese örtlichen Unterkühlungen wurden algebraisch gemittelt, um die Volumenunterkühlung zu erhalten.

Aus den experimentellen Ergebnissen wurden die Wachstums- und Keimbildungsgeschwindigkeiten berechnet. Durch Vergleich der experimentellen mit den mit Hilfe eines mathematischen Modells berechneten Wachstumsgeschwindigkeiten ist die Kinetik des Einbaus von Wassermolekülen in das Gitter des Eises bestimmt worden. Es ergab sich, daß die Wachstumsgeschwindigkeiten der Grenzflächenunterkühlung direkt proportional sind. Die Geschwindigkeitskonstante nimmt mit zunehmenden Gewichtsprozenten der Dextrose in der Lösung exponentiell ab.

Die Keimbildungsgeschwindigkeit wurde als direkt proportional der Gesamtkristalloberfläche pro Volumeneinheit der Suspension und proportional der 2,1. Potenz der Volumenunterkühlung gefunden. Es wird angenommen, daß die Keimbildung durch den Abrieb von Dendriten von der Oberfläche der Primärkristalle erfolgt.

[1]) Paper presented on the 5th Symposium on Industrial Crystallization, Chisa Congress Prague 1972.

1. Introduction

Crystallization of ice from aqueous solutions is studied widely, especially for its application in solute concentration and water purification processes. Knowledge of the kinetics of nucleation and growth of ice crystals from aqueous solutions is a prerequisite for optimal crystallizer and separator design. The specific surface of the crystals produced in the crystallizer determines the efficiency and the rate of separation of concentrated liquid from ice. This total crystal surface per unit volume of ice, that will be expressed by the effective diameter d_e, is mainly influenced by the growth rates, and by the mean residence time and residence time distribution of the crystals.

Experiments have been performed in a continuously operated, well mixed, adiabatic vessel with supercooled feed. The effective diameter of the product crystals has been determined for various operating conditions. Nucleation and growth rates that are calculated from the experimental data are correlated with internal system variables, such as total crystal area per unit volume, bulksupercooling, and the energy dissipated by the impeller per unit mass of suspension. By means of these general correlations heat and mass balances, and a population balance, the average crystal size and moments of the crystal size distribution can be calculated for various types of crystallizers (Larson, Randolph; Hulburt, Stefango).

2. Theoretical

2.1. Growth rate

Ice crystals growing freely from supercooled aqueous solutions usually exhibit a disk-like shape (Lindenmeijer, Chalmers). The growth of these ice crystals can be described by two linear growth rates along the main crystallographic axes. These linear growth rates are not the same due to different inbuilding kinetics in both crystallographic directions.

In addition to the inbuilding kinetics, the linear growth rate is also dependent upon the rates of heat and mass transfer between the crystal interface and the bulk of the solution. The heat and mass transfer coefficients can be calculated from the power input ε, of the impeller per unit mass of suspension, the linear crystal size l and appropriate physical constants. From the experimental data reported by Brian, Hales and Sherwood and the effects of the volume fraction ζ upon heat and mass transfer coefficients (Rowe, Claxton), the following correlations could be derived:

$$Nu = 2/(1-\zeta^{1/3}) + \left(1.3/(1-\zeta)\right)(\varepsilon\, l^4/\nu^3)^{.17}\, Pr^{.25} \text{ for } (\varepsilon\, l^4/\nu^3) < 10^6 \quad (1)$$

and

$$Nu = 2/(1-\zeta^{1/3}) + \left(0.4/(1-\zeta)\right)(\varepsilon\, l^4/\nu^3)^{.243}\, Pr^{.25} \text{ for } (\varepsilon\, l^4/\nu^3) < 10^6$$

in which Nu is the Nusselt number for heat or mass transfer, Pr is the Prandtl number for heat transfer or the Schmidt number for mass transfer, and ν is the kinematic viscosity.

For the calculation of the linear growth rate in one crystallographic direction the linear ice crystal size in the other direction is taken as the characteristic length l for heat and mass transfer (equation (1)). The heat transfer coefficient h is calculated from a heat balance:

$$v(l) = h\,(T_i - T_b)/\Delta H\, \varrho_s\,, \quad (2)$$

in which T_i is the interface temperature, $v(l)$ is the linear growth rate, ΔH is the enthalpy of crystallization, and ϱ_s is the specific weight of ice. Since no dextrose molecules are built into the ice lattice a dextrose mass balance yields:

$$v(l)\, C_i\, \varrho_s/\varrho = k\,(C_i - C_b)\,, \tag{3}$$

where C_i and C_b are dextrose concentrations at the interface and in the bulk respectively, ϱ is the specific weight of the solution and k is the mass transfer coefficient. C_i and C_b can be related to their respective equilibrium temperatures T_i^* and T_b^*. The overall driving force $T_b^* - T_b$ will be referred to as the bulksupercooling.

For ice crystals growing dendritically in flowing water at supercoolings between 0.1 and 0.5 °C, the inbuilding kinetics for the fastest growing direction (a-direction) have been expressed by HUIGE and THIJSSEN:

$$v_a = 0.27\, \Delta T_i^{1.55}\,, \tag{4}$$

in which ΔT_i is the interface supercooling. In applying eq. (4) to growth of ice crystals in dextrose solutions, the interface supercooling ΔT_i can be written as $T_{il}^* - T_i$.

T_{il}^* is the equilibrium temperature of a dextrose solution with concentration C_i in equilibrium with a crystal of size l. The freezing point depression $T_i^* - T_{il}^*$ is given by the Gibbs-Thomson equation:

$$T_i^* - T_{il}^* = \frac{4\,\sigma\, T_i^*}{l\,\Delta H\,\varrho_s}\,, \tag{5}$$

in which σ is the surface free energy and T_i^* is the freezing point of the solution at the interface.

Relationships similar to eq. (4) have been published for both the fastest (SHERWOOD, BRIAN) and slowest directions (MICHAELS, BRIAN, SPERRY; KETCHAM). The correlations for the slowest growing direction (c-direction) are commonly second order in the interface supercooling ΔT_i:

$$v = 0.027\, \Delta T_i^2\,. \tag{6}$$

A second order dependency can be expected for an inbuilding mechanism in which dislocations serve as growth steps (HILLIG, TURNBULL). By means of the equilibrium data and physical constants, and for known values of the supercooling, l, ε, and ζ, $v(l)$ can be calculated iteratively from equations (1) through (5).

2.2. Nucleation

In a continuously operated crystallizer nucleation is most likely caused by suspended crystals. This type of nucleation, usually referred to as secondary nucleation, takes place at much smaller supercoolings than nucleation in a crystal free solution. Secondary nucleation can occur by several mechanisms:

1. nucleation by breakage of dendritical growths from the crystal surface;
2. nucleation by shearing off parts of a structured layer at the surface of parent crystals;
3. nucleation by mechanical breakage of parent crystals.

ad. 1. Crystals can grow dendritically when the supercooling exceeds a critical value. Ice crystals are observed to grow as very thin platelets and surface

needles even at supercoolings as low as 0.5 °C([3]). The growth rate of the dendritic protuberances and therefore the probability of breakage increases with increasing supercooling. Furthermore the chance that a broken off dendrite becomes a stable nucleus increases with increasing supercooling. The rate of nucleation due to this mechanism is linearly dependent on the crystal surface, since the number of sites available for dendritic growth is determined by that crystal surface.

ad. 2. Water molecules that are transported to the crystal surface are not built into the crystal lattice immediately, since at supercoolings smaller than 9 °C inbuilding of these molecules only takes place at preferred locations at the crystal surface. An adsorption layer is therefore formed around the crystals. In this layer the water molecules have a more ice-like structure than in the bulk. If parts of this adsorption layer are torn away from the surface, these fragments may become stable nuclei, depending on the supercooling, the size of the fragment, and the molecular concentration of the fragment. The rate of nucleation due to this mechanism increases with the number and size of the fragments that are sheared off. The nucleation rate increases therefore with increasing total volume of the adsorption layer and consequently with the total crystal surface.

The separation of prenuclei from the parent crystal can occur by:

1. fluid shear (applicable to mechanismus 1 and 2),
2. collision of crystals with the impeller, fixed surfaces in the crystallizer or with other crystals (applicable to all three mechanisms).

If the forces extered by fluid shear are not large enough, breakage can only be caused by collision. For nucleation caused by collision it has been shown that the nucleation rate is linearly proportional to the impact energy (CLONTZ, MCCABE).

The rate of nucleation by crystal-crystal collision is linearly proportional to the power input (ε) of the impeller per unit mass of suspension and to the square of the total mass of crystals per unit volume (M).

For nucleation resulting from collisions of crystals with fixed surfaces or the impeller the rate increases linearly with ε and M (OTTENS, JANSE, DE JONG).

2.3. Crystal size distribution

For a mathematical description of crystallization processes not only energy and material balances must be considered, but also an additional conservation law is needed for a complete description of the crystal size distribution. For this conservation law the population density balance will be used. This balance can be expressed by the following partial differential equation (LARSON, RANDOLPH):

$$\frac{\delta n(l)}{\delta t} + \frac{\delta(v(l)\, n(l))}{\delta l} = \frac{-n(l)}{\tau} + B(l) - D(l)\,, \tag{8}$$

where $n(l)$ is the population density, t is the time and τ is the mean residence time of the ice crystals. $B(l)$ and $D(l)$ indicate respectively the increase and decrease of the number of crystals in a size interval $(l, l + \Delta l)$ due to breakage. The population density is defined by:

$$n(l) = \lim_{\Delta l \to 0} \frac{\Delta N}{\Delta l}$$

in which ΔN is the number of crystals per unit volume of suspension in the size interval $(l, l + \Delta l)$.

In the derivation of eq. (8) the following assumptions are made:

— constant suspension volume;
— ideally mixed suspension;
— no agglomeration.

If nucleation only occurs by mechanisms 1 and 2 eq. (8) reduces for steady state conditions to:

$$\frac{d(n(l)\, v(l))}{dl} = -\frac{n(l)}{\tau}. \tag{9}$$

The size distribution is usually characterized by its moments. The i^{th} moment is defined as:

$$\mu_i = \int_0^{\sim} n\,(l)\, l^i\, dl \qquad i = 0, 1, \ldots, N. \tag{10}$$

The shape of the crystals can be characterized by the shape factors $k\,a$ and $k\,v$, that can be calculated from:

$$A = k\,a\,l^2 \quad \text{and} \quad V = k\,v\,l^3 \tag{11}$$

where V is the volume and A is the surface of one crystal with a linear size l. For shape factors, that are independent of crystal size and supercooling, the total surface and volume of the crystals per unit volume of suspension are given by respectively $(k\,a\,\mu\,2)$ and $(k\,v\,\mu\,3)$.

3. Experimental

3.1. Description of the apparatus

The experimental set-up is schematically indicated in Figure 1. From a storage tank a crystal free solution, that is kept a few degrees above its freezing point, is pumped through a heat exchanger to a crystallizer with a volume of 2 liters. In the heat exchanger the solution is cooled to the desired supercooling. The crystallizer is provided with a three bladed propellor in an offcenter position. In order to be able to vary the magma density independently of the feed supercooling, both a product suspension stream and a crystal free solution are withdrawn from the crystallizer. The crystal free solution is pumped to the storage tank.

The suspension is withdrawn semi-continuously by means of a pipe that can be moved in and out of the suspension by means of a motor. This pipe is connected to a vacuum system. The dip frequency is controlled by a level indicator that operates the motor. By means of this system the suspension volume in the crystallizer can be kept constant within 2.5%. After the ice crystals in the suspension have melted in a heat exchanger, the solution flows to the tank. To compensate for the energy of mixing the crystallizer is externally cooled by means of a cooling mantle, such that it works adiabatically at the desired operating conditions.

3.2. Crystal size measurement

The effective crystal diameter d_e is defined as the diameter of a sphere with the same specific surface as the crystals:

$$d_e = \frac{6}{Sp}. \tag{12}$$

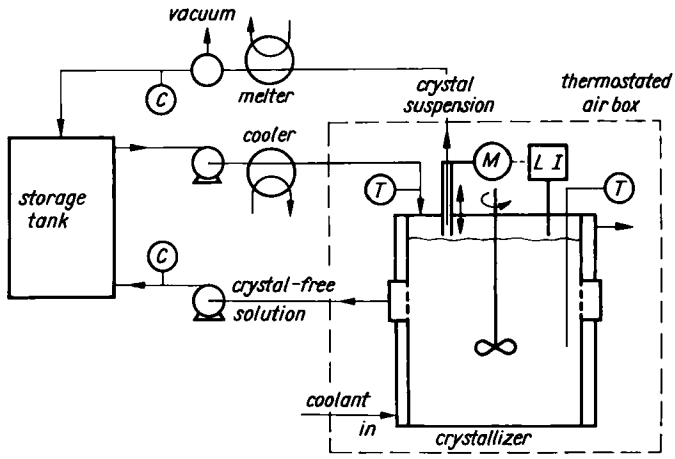

Fig. 1. Experimental set-up

The specific surface of the ice crystals can be calculated by means of the Carman-Ergun equation from the permeability K and the porosity e of a packed bed made from the product crystals; for $Re < 5$:

$$K = \frac{e^3}{(1-e)^2\, 5\, Sp^2}. \tag{13}$$

The porosity is determined from the dextrose concentration of the filtrate C_f and the overall dextrose concentration of the bed C_{bed}. This overall concentration of the bed is the value obtained once the bed, filled with filtrate, is melted.

$$e = \left[1 + \left(\frac{C_f}{C_{bed}} - 1\right)\frac{\varrho_f}{\varrho_s}\right]^{-1}$$

In this equation ϱ_s and ϱ_f are the specific weights of respectively ice and filtrate.

For laminar flow ($Re < 5$) through packed beds the permeability can be calculaetd from Darcy's law:

$$K = \frac{u\,\mu\,H}{\Delta P},$$

in which μ is the viscosity, u is the superficial velocity of the filtrate, H is the height of the bed and ΔP is the pressure drop over the bed.

The value of 5 in eq. (13) is the most commonly used value for the permeability constant k'. Theoretically k' depends on the shape of the particles and the tortuosity of the pores in the bed. COULSON measured permeabilities of beds with particles of different shapes and sizes. He found values of k' between 3.4 and 5.8, but did not find any dependency of k' on the shape or size of the particles. It has also been suggested (SHERWOOD, BRIAN) that k' should be dependent on the particle size distribution. Experiments in our laboratory with glass beads of various size distributions, however, showed k' to be independent of the particle size distribution.

3.3. Crystal shape measurements

In order to determine the shape of the product crystals, representative samples of the suspension at steady state conditions were placed under a microscope and photographed. To prevent melting or growing of the crystals the microscope was placed in a thermostated air box that was kept within 0.1 °C of the freezing point of the suspension.

3.4. Supercooling measurements

Temperatures of feed stream and suspension are measured by means of an N. T. C. thermistor. The feed supercooling is defined as the difference between the suspension temperature and the temperature of the feed stream. The suspension supercooling is measured from the temperature increase in the suspension after the feed stream is stopped. The supercooling of the suspension is measured at 9 different locations in the crystallizer. The bulksupercooling ΔT_b is calculated by averaging the local mean supercoolings. With the N. T. C. thermistor, temperature differences can be measured with an inaccuracy of about 10^{-3} °C.

3.5. Experimental results

The effective crystal diameter and the bulksupercooling have been measured for various combinations of the following independent variables: C_b, τ, feed supercooling ΔT_f, volumetric feed rate Φ_f, and the impeller speed nr. The ranges in which these operating variables are varied are given in Table 1.

Table 1
Operating variables

variable	varied between
ΔT_f	1—2 °C
Φ_f	0.5—8 $cm^3 \cdot s^{-1}$
τ	400—4000 s
C_b	10—42 wt %
$n\,r$	15—27 rps

The measurements of d_e were always carried out at a time larger than $3\,\tau$ after the onset of the experiment. Calculations that were carried out to determine the variation of the crystal size distribution with time showed that in many cases values of d_e at $3\,\tau$ were within 10% of the steady state values, although the distribution would still become considerably wider after $3\,\tau$. The results of these calculations depended however, upon the initial conditions which cannot be known. By determining the steady state value of d_e after $3\,\tau$ probably only a minor error is made due to the omission of the largest crystal sizes that would have been found at times $> 3\,\tau$.

The results are compiled in Table 2. The run-number is indicated in column 1. The independent variables ΔT_f, Φ_f, τ, C_b, and $n\,r$ are given in the columns 2 through 6 respectively . The weight fraction of crystals X is calculated from a heat balance over the adiabatic crystallizer:

$$\Delta T_f\,\Phi_f\,\varrho_f\,c_{pf} = \varrho_{susp}\,X\,V\,\Delta H/\tau = Q\,, \tag{14}$$

in which c_{pf} is the specific heat of the feed solution and V is the total suspension volume. X has also been determined directly by measuring the dextrose concen-

Table 2
Experimental results of ice growth in dextrose solution

nrs	ΔT_f (°C)	Φ_f (cm³ · s⁻¹)	τ_{ice} (s)	C_b (wt %)	nr (rps)	X (wt %)	d_e (cm)	ΔT_b (°C)	$ka\,\mu_s$ (cm⁻¹)	J (cm⁻³ · s)
1	2.4	4.15	2857	27.3	20	15.9	.0222	.010	50.5	20.1
2	2.05	10.1	606	26.3	20	7.3	.0112	.0225	46.7	344
3	2.05	3.2	4651	27.6	20	16.9	.0235	.0070	50.6	11.0
4	2.3	3.5	1111	26.0	20	5.4	.0122	.0165	31.8	108
5	2.3	3.1	615	26.0	20	2.5	.0100	.0250	18.1	157
6	2.15	.65	3077	25.9	20	2.3	.0179	.008	9.3	5.3
7	2.15	1.2	3921	26.3	20	6.1	.0204	.0085	21.5	7.4
8	2.15	2.4	3922	27.0	20	10.5	.0212	.012	25.3	11.2
9	2.0	7.1	676	24.7	20	4.9	.0134	.025	26.3	121
10	2.0	8.4	760	25.0	20	7.1	.0159	.0225	32.0	93.2
11	1.0	5.35	769	24.3	20	3.4	.0138	.0227	17.7	68.0
12	0.9	5.2	1156	26.3	20	3.0	.0151	.017	14.3	32.0
13	0.9	8.2	1333	26.3	20	5.0	.0177	.0165	20.3	27.2
14	1.1	5.3	3125	27.2	20	9.9	.0232	.0093	30.4	10.1
15	1.0	5.1	2381	26.1	20	6.5	.0218	.0084	21.4	10.6
16	.95	7.2	2899	25.6	20	10.3	.0250	.0093	29.3	9.0
17	.8	1.8	3922	25.0	20	3.0	.0185	.0065	11.7	4.9
18	2.2	5.0	1770	29.1	20	9.7	.0168	.0181	41.2	46.2
19	2.0	5.0	2000	29.7	20	9.8	.0194	.0170	36.0	26.8
20	2.0	5.1	840	29.6	15	4.5	.0109	.0321	29.7	167
21	1.0	5.0	820	29.2	15	2.1	.0092	.0321	16.5	133
22	2.0	1.5	1626	29.2	15	2.2	.0191	.0187	8.3	7.9
23	1.7	4.9	830	29.5	15	3.4	.0113	.0378	21.7	115
24	2.1	1.1	2326	29.7	15	2.5	.0146	.0147	12.4	14.0
25	2.0	1.1	2273	30.1	15	2.3	.0166	.0189	10.0	9.0
26	2.0	5.1	580	30.6	15	3.0	.0094	.060	23.0	252
27	2.2	1.1	1818	29.1	15	2.3	.0168	.0178	9.9	10.8
28	2.0	1.15	2632	29.5	15	3.3	.0196	.0122	13.1	6.7
29	2.0	2.3	1124	30.0	15	2.9	.0108	.0250	19.4	82.8
30	2.0	7.2	641	29.7	15	4.9	.0100	.0411	35.2	306
31	2.0	3.7	1667	29.0	27	6.6	.0155	.0217	30.5	42.4
32	2.1	5.0	441	28.3	27	2.2	.0108	.0363	14.7	160
33	2.0	2.1	1818	28.9	27	3.9	.0143	.0141	19.6	29.6
34	1.9	7.25	935	29.0	27	6.5	.0125	.0233	37.3	143
35	2.0	7.7	426	28.8	27	3.5	.0088	.0386	28.7	486
36	2.1	2.1	962	29.3	27	2.2	.0125	.0238	12.7	47.4
37	2.1	5.0	800	29.7	27	4.2	.0136	.0256	22.2	84.2
38	1.0	7.3	1575	29.7	27	5.4	.0165	.0167	23.5	30.7
39	1.0	7.4	794	29.7	27	2.8	.0122	.0251	16.5	78.5
40	1.0	4.9	1481	29.7	27	3.9	.0158	.0161	17.8	26.9
41	1.0	5,4	1290	29.7	27	3.6	.0155	.0158	16.7	30.3
42	1.0	4.2	1111	29.6	27	2.2	.0130	.0235	13.2	36.5
43	1.0	2.1	1852	29.8	27	1.9	.0130	.0181	10.5	18.9
44	1.8	4.6	1550	41.3	20	5.7	.0106	.030	40.3	130
45	2.0	4.6	1332	41.6	20	6.0	.0096	.033	47.0	216
46	0.8	4.2	2380	41.3	20	3.1	.0115	.021	20.3	35.2
47	1.1	4.0	2700	42.0	20	5.6	.0144	.020	29.3	29.4
48	0.9	6.0	3120	10.2	20	7.0	.0350	.006	13.6	2.0
49	1.1	6.5	1200	10.6	20	5.5	.0289	.011	12.9	7.2

tration of the crystal free solution and of the suspension after melting. The values of X determined by the two methods are averaged and compiled in column 7. The mean deviation from the average values is 6%. The d_e measurements for most runs are carried out in duplicate. The average values of d_e are indicated in column 8. The mean deviation from the average values is 2.9%.

The bulk supercooling is indicated in column 9. The total crystal surface per unit volume of suspension $k\,a\,\mu\,2$ is calculated from:

$$k\,a\,\mu\,2 = 6\,X\,\varrho_{susp}/(d_e\,\varrho_s)\,. \tag{15}$$

Values of $k\,a\,\mu\,2$ are given in column 10.

From representative samples of crystals obtained in the runs 35, 39, and 40 crystal shape factors have been determined. The crystals appeared to have the shape of flat disks. The height over diameter ratio f was approximately constant for the crystals from all three runs. The average value of f was found to be 0.26, as is indicated in Figure 2. For the calculations the shape factors $k\,a$

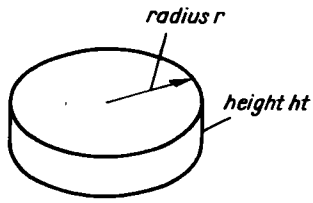

Fig. 2. Shape of ice crystals assumed for the calculations for ice growth in dextrose solutions. $f = ht/2\,r = 0.26$

and $k\,v$, as defined in eq. (11), will be related to the disk radius r. This yields 9.56 and 1.64 for $k\,a$ and $k\,v$ respectively.

The experimental data will be plotted versus various operating variables in the following figures. For the sake of clearness these data will be lumped into groups that will each be indicated in the figures by means of one symbol. The following groups have been distinguished: runs 1—17 ($\overline{C}_b = 26.0$, $n\,r = 20$), runs 18 and 19 ($\overline{C}_b = 29.4$, $n\,r = 20$), runs 20—30 ($\overline{C}_b = 29.7$, $n\,r = 15$), runs 31—43 ($\overline{C}_b = 29.5$, $n\,r = 27$), runs 44—47 ($\overline{C}_b = 41.5$, $n\,r = 20$), and runs 48 and 49 ($\overline{C}_b = 10.4$, $n\,r = 20$).

In Figure 3 the effective crystal diameter is plotted versus the mean crystal residence time. The parameters in this graph are the impeller speed and the weight percentage of ice in the crystallizer (indicated for every data point). The effects of Φ_f and ΔT_f appeared not to be significant and these parameters are therefore not indicated. Notwithstanding the scatter in data points it can be concluded from Figure 3 that d_e increases less than linearly with increasing τ. Furthermore d_e seems to increase slightly with increasing X. It can also be concluded that at constant τ and $n\,r$, d_e increases with decreasing C_b. From the data for $n\,r = 15$ and $n\,r = 27$ it can be seen that d_e seems to decrease with decreasing $n\,r$.

In Figure 4 the bulk supercooling is plotted versus τ, with $n\,r$ and C_b as parameters. The influences of Φ_f, ΔT_f, and X upon the relationship between ΔT_b and τ are negligible. Figure 4 clearly shows that ΔT_b increases with decreasing τ. By comparing the data points for $n\,r = 27$ and $n\,r = 15$ at constant C_b and τ it can be seen that ΔT_b increases only slightly with decreasing $n\,r$. From the data for $n\,r = 20$ it can be seen that ΔT_b increases considerably with increasing C_b.

3.6. Growth kinetics

The total volume of ice crystals that is produced per unit time and per unit crystallizer volume can be expressed by:

$$\frac{k\,v\,\mu_3}{\tau} = c_1 \int_0^{\tilde{}} v(l)\,n(l)\,l^2\,dl\,, \tag{16}$$

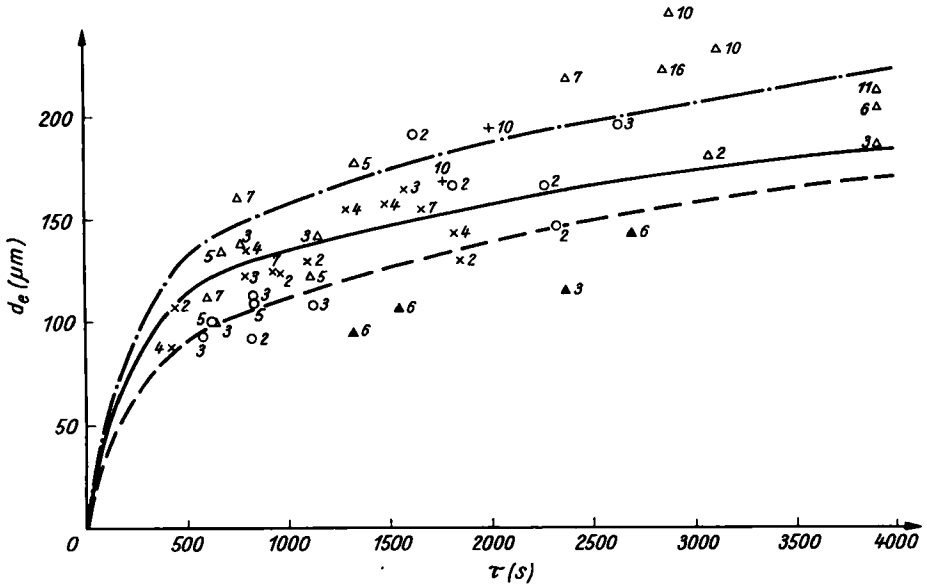

Fig. 3. Effective crystal diameter versus mean crystal residence time with weight percentage of ice as a parameter. parameter X (wt %).

	nr	$\bar{C}_b$	nr	$\bar{C}_b$
– – –	○ 15	29.7	+ 20	29.5
·–·–·	△ 20	26.0	▲ 20	40.5
———	× 27	29.5		

in which c_1 is a constant depending upon the particle shape. For the following calculations the growth rate, moments of the size distribution, and shape factors will be defined in terms of the disk radius r. For a disk shaped crystal with a constant height over diameter ratio of 0.26, c_1 equals 4.9. For comparison between theory and experiments an area averaged growth rate in the fastest growing direction (indicated by subscript a) $\bar{v}_a$ is defined:

$$\bar{v}_a = \int_0^{\tilde{}} v_a(r)\, n(r)\, r^2\, dr \Big/ \int_0^{\tilde{}} n(r)\, r^2\, dr\,. \tag{17}$$

Equation (16) can then be transformed to:

$$k\, v\, \mu_3 = c_1\, \bar{v}_a\, \mu_2\, \tau\,.$$

From the definition of the effective diameter d_e (eq. 12) a simple expression for $\bar{v}_a$ can be derived:

$$\bar{v}_a = d_e/(3.04\,\tau)\,. \tag{18}$$

From the experimental data values of $\bar{v}_a$ have been calculated by means of eq. (18). The results are plotted versus the bulksupercooling in Figure 5. The parameters in this graph are the stirring rate and the weight percentage of dextrose. From Figure 5 it can be seen that the area averaged growth rate is approximately linearly proportional to the bulksupercooling. Furthermore $\bar{v}_a$ i ncrease

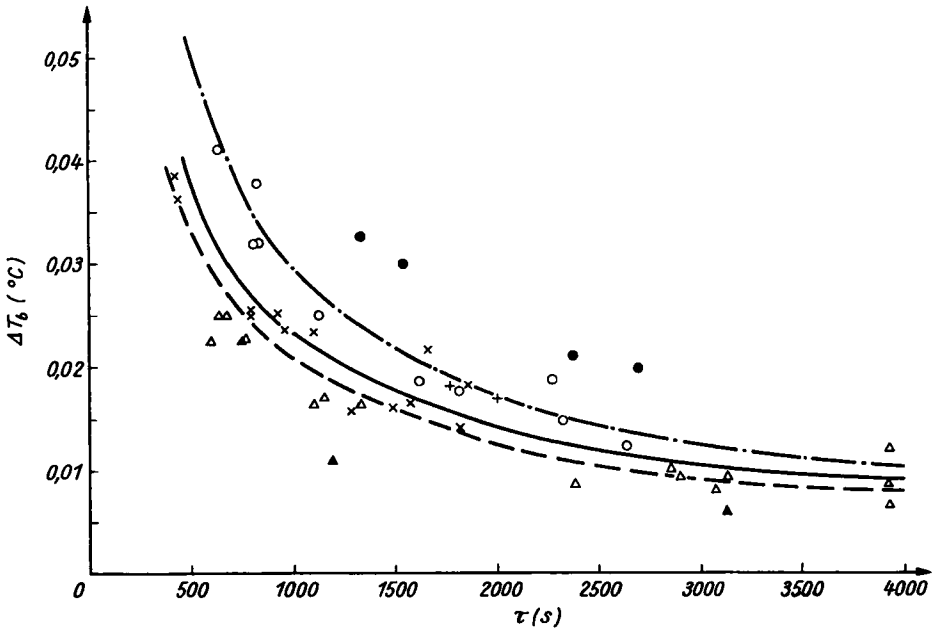

Fig. 4. Bulk supercooling versus mean crystal residence time.

	nr	$\bar{C}_b$	nr	$\bar{C}_b$
·-·-·-	○ 15	29.7	+ 20	29.5
– – –	△ 20	26.0	▲ 20	10.4
———	× 27	29.5	● 20	40.5

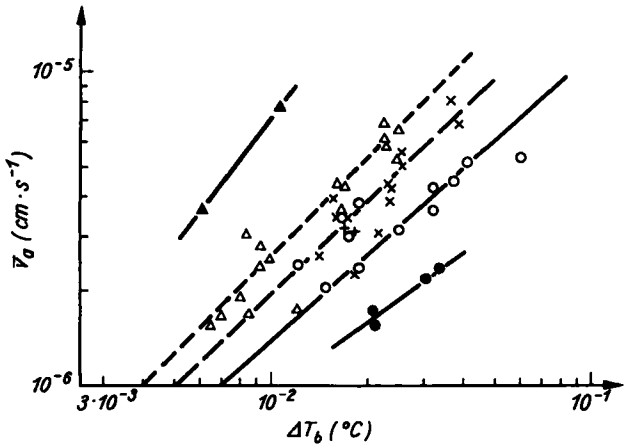

Fig. 5. Experimentally determined area averaged growth rates of ice in dextrose solutions as a function of bulk supercooling.

nr	$\bar{C}_b$	nr	$\bar{C}_b$
○ 15	29.7	+ 20	29.5
△ 20	26.0	▲ 20	10.4
× 27	29.5	● 20	40.5

with increasing stirring rate and with decreasing dextrose concentration. From the experimental data the following correlations can be determined:

$$\left.\begin{aligned} \bar{v}_a &= 0.91_{10^{-4}}\ \Delta T_b^{0.91} \quad \text{for} \quad n\,r = 15,\ \bar{C}_b = 29.7 \\ \bar{v}_a &= 2.95_{10^{-3}}\ \Delta T_b^{1.03} \quad \text{for} \quad n\,r = 20,\ \bar{C}_b = 26.0 \\ \bar{v}_a &= 1.73_{10^{-3}}\ \Delta T_b^{0.97} \quad \text{for} \quad n\,r = 27,\ \bar{C}_b = 29.5 \end{aligned}\right\} \tag{19}$$

These experimentally determined growth rates will now be compared to theoretical values of the area average growth rates. Therefore the integrals of eq. (17) are calculated numerically after solving the population density balance, eq. (9). These calculations are carried out for every experiment. The linear growth rate $v_a = v_a(r)$ in eq. (9) is calculated from eqs. (1), (2), (3), (5), and inbuilding kinetics relationship eq. (4) for ice dendrites growing in flowing water.

The theoretical values of $\bar{v}$ appeared to be a factor of 5 larger than the experimental values. Harriott, and Sherwood, Brian also found that experimentally determined growth rates of suspended crystals growing from salt solutions were a factor of 2 to 10 lower than theoretically predicted ones. They attributed these differences to an appreciably higher inbuilding resistance than would be predicted from other literature sources. The discrepancy between theoretical and experimental values can most likely be attributed to the very speculative use of the inbuilding kinetics relationship eq. (4). For growth of ice crystals in dextrose solutions a different inbuilding kinetics relationship can be expected for a number reasons:

1) Dextrose molecules at high concentration may increase the inbuilding resistance considerably by preferential adsorption at growth sites and by decreasing the rate of surface diffusion.
2) In the stirred vessel partial melting of crystals may occur occasionally in areas of small supercooling. Partial melting of crystals can give rise to surface pitting. Dislocations that are formed this way cause the inbuilding resistance to decrease.
3) Eq. (4) was determined for supercoolings between 0.1 and 0.5 °C. The supercoolings in the stirred vessel are in the order of 0.005 to 0.05 °C.
4) The hydrodynamic conditions around freely suspended crystals in a stirred vessel are quite different from those of forced convection around a fixed dendritically growing ice crystal. In a stirred vessel dislocations might arise from collisions of crystalls with the stirrer or with each other. Due to this effect the inbuilding resistance for growth in stirred vessels can be expected to be be lower than for growth of a fixed dendritical crystal.

It was therefore attempted to obtain a good fit between experimental and theoretical growth rates by varying in the theoretical calculations the expression for the inbuilding kinetics. A general expression is used of the form:

$$v = k\,r\ \Delta T_i^p\,. \tag{20}$$

By means of trial and error it has been found that the best agreement between all experimental and theoretical growth rates is obtained for a value of the exponent $p = 1$ and a concentration dependency of the inbuilding rate constant $k\,r$. The values of $k\,r$ for which the best fit between experimental and theoretical growth rates are obtained are given in Table 3 together with the appropriate values of $n\,r$ and C_b. The number of experiments that have been used to obtain

Table 3

Values of the rate constant $k\,r$ for first order inbuilding kinetics

$k\,r$ (cm · s^{-1})	$n\,r$ (rps)	C_b (wt %)	number of exps.
$0.15_{10^{-4}}$	15	29.7	11
$0.26_{10^{-4}}$	20	26.0	17
$0.20_{10^{-4}}$	27	29.5	13
$0.69_{10^{-4}}$	20	10.4	2
$0.18_{10^{-4}}$	20	29.4	2
$0.82_{10^{-4}}$	20	41.5	4

these average $k\,r$ values is indicated in the last column. In Figure 6 the experimentally determined area averaged growth rates are compared to the theoretical ones calculated with the values of $k\,r$ from Table 3. From the data in Table 3 it can be seen that the inbuilding resistance increases slightly with decreasing $n\,r$. The effect of dextrose concentration on $k\,r$ is graphically represented in Figure 7 on a semi-logarithmic scale. The relationship between $k\,r$ and C_b for $n\,r = 20$ can be approximated by:

$$k\,r = 1.45_{10^{-4}}\, exp^{-0.03\, C_b}\,. \tag{21}$$

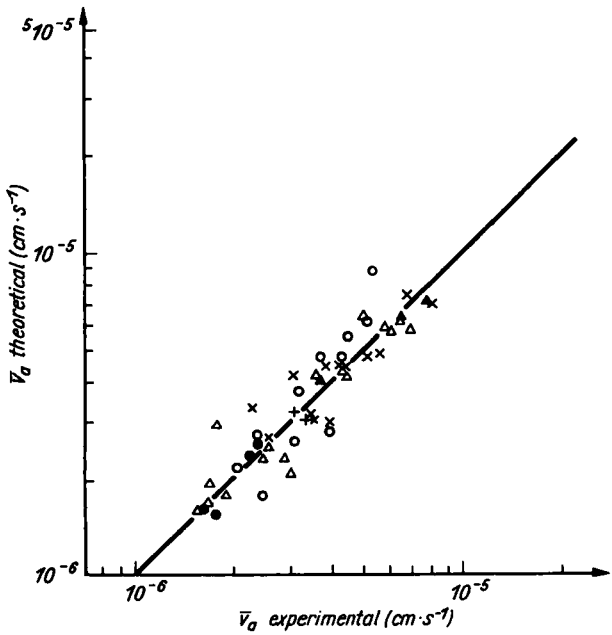

Fig. 6. Comparison between experimental and theoretical area averaged growth rates of ice in dextrose solutions.

nr	$\bar{C}_t$	nr	$\bar{C}_b$
○ 15	29.7	+ 20	29.5
△ 20	26.0	▲ 20	10.4
× 27	29.5	● 20	40.5

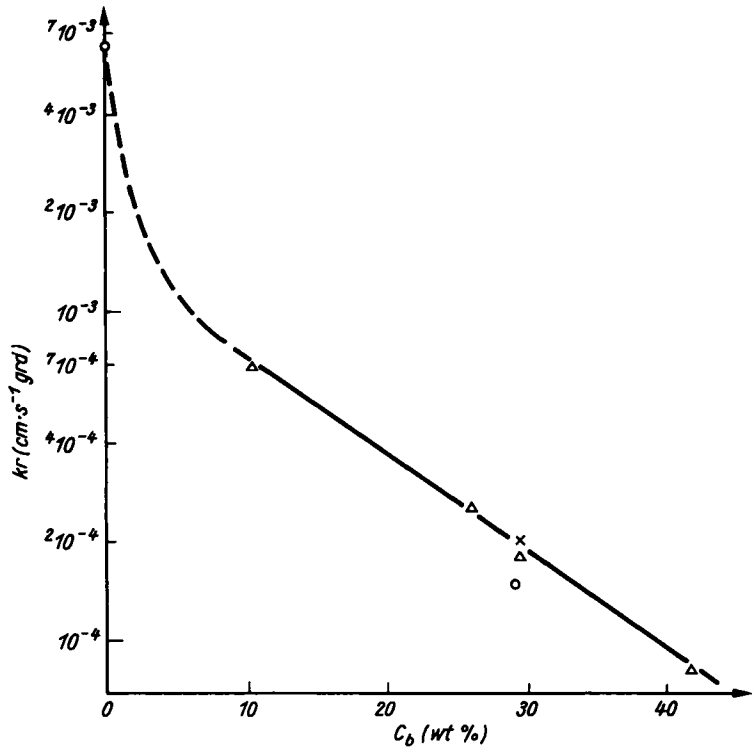

Fig. 7. Influence of dextrose concentration upon rate constant for first order kinetics. $v_a = k\,r\,\Delta T_i$ ○ $nr = 15$; △ $nr = 20$; × $nr = 27$

From this equation it follows for the linear growth rate in the a-axis direction:

$$v_a = 1.45_{10^{-4}}\, exp^{-0{,}03\ C_b}\, \Delta T_i\,. \tag{22}$$

The increase of $k\,r$ with increasing C_b can be explained in a number of ways:

- if dextrose molecules adsorb at growth sites, increasing C_b yields a smaller fraction of the total area available for growth;
- increasing the dextrose concentration decreases the diffusion coefficient of water molecules at the interface, and consequently decreases the rate of surface diffusion;
- with increasing C_b the relaxation time for inbuilding of water molecules increases. This relaxation time is the time that is necessary for water molecules to break away from their liquid structure in which certain intermolecular forces between water and dextrose molecules exist.

It has to be remarked that inbuilding kinetics relationship eq. (22) has been derived for growth in the a-axis direction. Because of the constant value of the shape factor f of 0.26 that is assumed, the inbuilding kinetics for the c-axis direction can be expressed by:

$$v_c = 0.46_{10^{-4}}\, exp^{-0.03\ C_b}\, \Delta T_i\,. \tag{23}$$

For ice crystals growing from pure water (HUIGE) the area averaged growth rates determined by means of the theoretical growth model using inbuilding kinetics relationship (4), are only 18% larger than the experimental values.

3.7. Nucleation kinetics

The net rate of nucleation J, i. e. the total number of crystals produced per unit volume and per unit time can be calculated from the following heat balance:

$$J\, k\, v\, \mu_3\, V\, \varrho_s\, \Delta H/\mu_0 = Q\,. \tag{24}$$

Since one would like to express $k\, v\, \mu_3/\mu_0$ in terms of de a linear relationship between $k\, v\, \mu_3/\mu_0$ and de is assumed:

$$k\, v\, \mu_3/\mu_0 = c_2\, d_e^3\,. \tag{25}$$

From the calculation of crystal size distributions by means of numerical integration of eq. (9) as described above, it appears that for every kinetic relationship that is used, c_2 is approximately constant for the entire range of experimental conditions. By using the inbuilding kinetic relationship eq. (22) an average value of $c_2 = 0.297$ results. The standard deviation from this value for runs 1 through 49 amounts to 0.012.

The valuess of J calculated by mean of eq. (23) and (25) and with $c_2 = 0.297$ are presented in the last column of Table 2.

In Figure 8 J is plotted versus τ for $n\,r = 27$ and $\overline{C_b} = 29.5$ with V as a parameter. J decreases strongly with increasing τ, while higher values of J are found at larger magma densities. Similar graphs are found for $n\,r = 20$ and $n\,r = 15$ rps. From these graphs the influence of $n\,r$ upon J is determined for various combinations of V and τ. The results are given in Figure 9.

It is evident from Figure 9 that the influence of the stirrer speed on J is much less then the influences of V and τ. The crystallization experiments that were

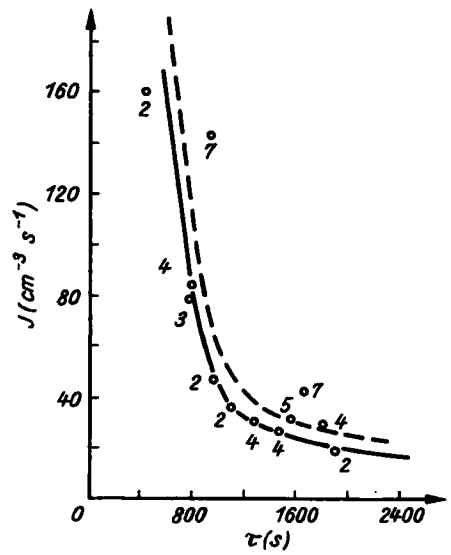

Fig. 8. Nucleation rate of ice crystals in 30 wt % dextrose solutions versus mean crystal residence time with weight percentage of ice as a parameter. $nr = 27$ (s^{-1}); ——— $X \simeq 3$; — — — $X \simeq 4.5$

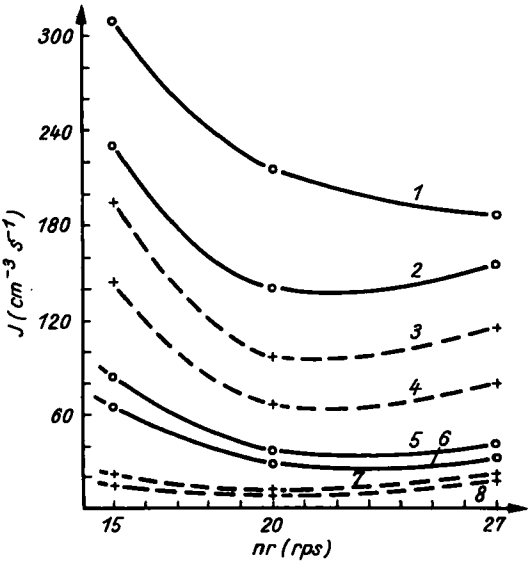

Fig. 9. Nucleation rate of ice crystals in dextrose solutions versus impeller speed with ice percentage and mean residence time as parameters.

	τ(s)	X(wt %)
1	600	4.5
2	600	3.0
3	800	4.5
4	800	3.0
5	1200	4.5
6	1200	3.0
7	2000	4.5
8	2000	3.0

carried out in our laboratory (HARRIOTT) with pure water showed a similar dependency of J on τ and X.

Theory predicts that the nucleation rate due to crystal breakage depends linearly on the power input of the impeller per unit mass of suspension. The power input is porportional to the impeller speed to the third power. From the minor influence of $n\,r$ on J that is found experimentally it can therefore be concluded that nucleation due to this mechanism can only have a small effect on the total number of crystals formed. The power required for nucleation due to shearing off dendrites or parts of a structured surface layer is much smaller than that required for breakage of crystals. It is possible therefore that already at the lowest shear forces that are encountered, a nucleation rate results that does not increase with further increase of the shear force as long as nucleation mechanism 3 does not occur. Nucleation of ice crystals from solutions at supercoolings in the order of 0.01 °C is not likely to occur by mechanism 2 since the size of a critical nucleus at these supercoolings is approximately 3.5 μm. If these nuclei would have been formed from parts of the adsorption layer or some other ordered layer around the crystal this layer would be in the order of 10^3 molecules thick.

Since for nucleation mechanism 1 the total crystal surface per unit volume of suspension and the bulksupercooling are important variables, a correlation of the following form will be used:

$$J = k\,n\,(k\,a\,\mu_2)^{m\,2}\,\Delta T_b^p\,. \tag{26}$$

For the equation: $ln\,J = m\,2\,ln\,(k\,a\,\mu_2\,\Delta T_b^{p/m\,2}) + \ln k\,n$ the best values $m\,2$ and $ln\,(k\,n)$ are calculated with the least square deviation method for various values of $p/m\,2$. The minimum value of the least square deviation is found for $p/m\,2 = 2{,}1$. This yields:

$$J = 7.82_{10^3}\,k\,a\,\mu_2\,\Delta T_b^{2.1}\,. \tag{27}$$

This correlation supports the presumption that nucleation takes place by mechanism 1, for which a linear dependence between K and $k\,a\,\mu_2$ can be expected.

By combining eqs. (12), (18), (19), and (27) relationships between d_e and τ and ΔT_b and τ can be derived. Knowledge of the value of c_1 is not necessary for this derivation. The results are:

$$\left.\begin{aligned} d_e &= 1.29_{10^{-3}}\,\tau^{0.312} \\ \Delta T_b &= 6.14\,\tau^{-0.773} \end{aligned}\right\} n\,r = 15\,,\ \overline{C}_b = 29.7$$

$$\left.\begin{aligned} d_e &= 2.87_{10^{-3}}\,\tau^{0.246} \\ \Delta T_b &= 2.8\,\tau^{-0.711} \end{aligned}\right\} n\,r = 20\,,\ \overline{C}_b = 26.0 \qquad (28)$$

$$\left.\begin{aligned} d_e &= 2.87_{10^{-3}}\,\tau^{0.223} \\ \Delta T_b &= 2.7\,\tau^{-0.688} \end{aligned}\right\} n\,r = 27\,,\ \overline{C}_b = 29.5$$

These relationships are drawn as solid lines in Figures 3 and 4. The curves seem to cover the data points reasonably well.

The fact that generally there is good agreement between eq. 28 and the data point justifies the lumping of data points that are used to obtain the general correlations.

References

Brian, P. L. T., Hales, H. R., Sherwood, T. K.: A. I. Ch. E. Journal **15**, 727 (1969)

Clontz, N. A., McGabe, W. L.: Chem. Eng. Propr. Symp. Ser. **67**, no. 110, 6 (1971)

Coulson, J. M.: Trans. Inst. Chem. Engrs. **27**, 237 (1949)

Harriott, P.: A. I. Ch. E. Journal **8**, 93 (1962)

Hillig, W. B., Turnbull, D.: J. Chem. Phys. **24**, 914 (1956)

Huige, N. J. J.: Thesis, Eindhoven, University of Technology, to be published May 1972

Huige, N. J. J., Thijssen, H. A. C.: Proc. Symp. Industrial Crystallization, London, April 1969, 69

Hulburt, H. M., Stefango, D. G.: Chem. Eng. Progr. Symp. Series **95**, no. 65, 50 (1969)

Ketcham, W. M.: J. Crystal Growth, **6**, 113 (1969)

Larson, M. A., Randolph, A. D.: Chem. Eng. Progr. Symp. Series **95**, no. 65, 1 (1969)

Lindenmeijer, C. S., Chalmers, B.: J. Chem. Phys. **45**, 2804 (1966)

Michaels, A. S., Brian, P. L. T., Sperry, P. R.: J. appl. Physics **87**, 4649 (1966)

Ottens, E. P. K., Jansen, H. A., de Jong, E. J.: to be published in J. Crystal Growth, 1972

Rowe, P. N., Claxton, K. T.: Trans. Inst. Chem. Engrs. **43**, T. 321 (1965)

Sherwood, T. K., Brian, P. L. T.: Res and Dev. Rept. no 474, U. S. Dept. of the Interior, Office of Saline Water, Washington 1970

(Received November 1, 1972; approved by the author January 19, 1973)

Authors' address:

Prof. H. A. C. Thijssen, Dr. N. J. J. Huige, Ir. M. M. G. Senden
TH Eindhoven
Laboratorium voor Fysische Technologie
Eindhoven
Insulindelaan 2
The Netherlands